Experimental and computational analysis of the combustion evolution in direct-injection spark-controlled jet ignition engines fuelled with gaseous fuels

A Boretti[1]*, **R Paudel**[1], and **A Tempia**[2]
[1]School of Science and Engineering, University of Ballarat, Ballarat, Victoria, Australia
[2]Robert Bosch (Australia) Pty Ltd, Clayton, Victoria, Australia

The manuscript was received on 15 December 2009 and was accepted after revision for publication on 4 May 2010.

DOI: 10.1243/09544070JAUTO1465

Abstract: Jet ignition and direct fuel injection are potential enablers of higher-efficiency, cleaner internal combustion engines (ICEs), where very lean mixtures of gaseous fuels could be burned with pollutants formation below Euro 6 levels, efficiencies approaching 50 per cent full load, and small efficiency penalties operating part load. The lean-burn direct-injection (DI) jet ignition ICE uses a fuel injection and mixture ignition system consisting of one main-chamber DI fuel injector and one small jet ignition pre-chamber per engine cylinder. The jet ignition pre-chamber is connected to the main chamber through calibrated orifices and accommodates a second DI fuel injector. In the spark plug version, the jet ignition pre-chamber includes a spark plug which ignites the slightly rich pre-chamber mixture which then, in turn, bulk ignites the ultra-lean stratified main-chamber mixture through the multiple jets of hot reacting gases entering the in-cylinder volume. The paper uses coupled computer-aided engineering and computational fluid dynamics (CFD) simulations to provide better details of the operation of the jet ignition pre-chamber (analysed so far with downstream experiments or stand-alone CFD simulations), thus resulting in a better understanding of the complex interactions between chemistry and turbulence that govern the pre-chamber flow and combustion.

Keywords: gas engines, direct injection, jet ignition, lean-burn stratified combustion, bulk ignition and combustion

1 INTRODUCTION

Development of more energy-efficient and environmentally friendly highway transportation technologies based on heavy-duty gas engines is a key factor for reducing fuel consumption, carbon dioxide (CO_2) production, and pollutants emissions within Australia, therefore improving national energy security, environment, and economy.

Up until the early 1960s, railways dominated all but the shortest land-based freight task. Since then, vast improvements in road vehicle productivity and road infrastructure quality, the gradual removal of regulations restricting road freight carriage, and the exponential growth in interstate trade has broadened the range of freight tasks for which road is more suitable than rail. The Australian domestic freight task measured 5.21×10^{14} t km in 2007, with 35 per cent carried by road [**1**], having road trains covering most of the interstate traffic.

Australia has the largest and heaviest road vehicles in the world, with some configurations topping out at close to 200 t. Two-trailer road trains, or B-doubles, are allowed in most parts of Australia, with the exception of some urban areas. Three-trailer road trains or B-triples operate in western New South Wales, western Queensland, South Australia, Western Australia, and the Northern Territory, with the last three states also allowing AB-quads (3.5 trailers). Road trains are used for transporting all manner of materials. Their cost-effective transport

*Corresponding author: School of Science and Engineering, University of Ballarat, PO Box 663, Ballarat, Victoria 3353, Australia.
email: a_boretti@yahoo.com

has played a significant part in the economic development of remote areas, with some communities totally reliant on a regular service.

The domestic freight task has doubled in size over the past 20 years, with an average growth of 3.5 per cent per annum. Bureau of Infrastructure, Transport and Regional Economics projections [**1**] suggest that this trend will continue, although with slightly slower growth into the future, growing by approximately 3.0 per cent per annum until 2030. Over this period, road freight volumes are projected to more than double, with domestic demand for manufactured goods sustaining much of the growth, even if the global financial crisis will certainly dampen freight growth in the near term. Australia's annual greenhouse gases emissions up to the 2009 June quarter for energy transport amount to 89 $MtCO_2e$ [**2**], or about 14.5 per cent of the total.

Life-cycle emissions analysis of alternative fuels for heavy vehicles [**3**, **4**] has shown the potential of gaseous fuels for heavy-duty trucks. There have been major advances in natural-gas engines in recent years, which means that the present generation of natural-gas vehicles has significantly lower emissions than the present generation of diesel vehicles. The emissions based on use in original equipment manufacturer (OEM) vehicles are lower in all categories, greenhouse gases, important criteria pollutants, and air toxics. The lower particulate matter (PM) emissions and noise levels compared with diesel make it particularly attractive for urban areas. The major uncertainty relates to upstream and in-service leakage, which have already been sufficiently reduced in the present generation of OEM natural-gas vehicles, and also to the lack of sufficient refuelling stations. The extra weight of compressed natural-gas (CNG) fuel tanks leads to slightly higher fuel consumption, or loss of payload in the case of buses, but this is less of a problem with liquefied natural-gas vehicles owing to the higher energy density.

Similarly, a dedicated liquefied petroleum gas (LPG) bus produces significantly lower emissions of important criteria pollutants, and lower exbodied emissions of greenhouse gases. Air toxics from tailpipe emissions of LPG vehicles are much lower than those of diesel vehicles, but the greater upstream emissions of air toxics causes the exbodied emissions of air toxics from LPG to be much the same as those from diesel. HD-5 grade LPG has a minimum propane (C_3H_8) content of 90 per cent whereas the ratio of C_3H_8 to butane (C_4H_{10}) varies widely in autogas LPG. When compared with autogas, HD-5 grade LPG emits more nitrogen oxides (NO_x) but less PM. Emissions of hydrocarbons (HCs) are similar. The main benefit of HD-5 grade LPG compared with autogas is that the compression ratio (CR) can be altered to suit this higher-octane fuel. The lower PM emissions and lower noise levels than with diesel make it attractive for use in urban areas. The major disadvantage of LPG is the lack of market penetration of dedicated heavy LPG vehicles.

Improving the efficiency of internal combustion engines (ICEs) is the most promising and cost-effective approach to increasing vehicle fuel economy in the next 10–20 years or until the time (which is still too far off to forecast) when plug-in hybrid electric or fuel cell hybrid vehicles will dominate the market [**5**]. Advanced combustion engines still have a great potential for achieving dramatic energy efficiency improvements in heavy-duty vehicle applications; the primary hurdles that must be overcome to realize increased use of advanced combustion engines are the higher cost of these engines, requiring expensive research and development compared with conventional engines, and compliance with particularly stringent new emission regulations with catalytic emission control technologies much less mature than gasoline engine catalysts.

Australian Standard ADR 80/03 requires compliance with Euro 5 standards for heavy-duty trucks starting 1 January 2010 for new model vehicles and 1 January 2011 for all produced vehicles. Near-future regulations will very probably follow Euro 6 standards. The Euro 6 regulation proposal will introduce particularly thorough emission standards [**6**]. Procedure provisions will be defined for test cycles, off-cycle emissions, particulate number, emissions at idling speed, smoke opacity, possible introduction of a nitrogen dioxide (NO_2) emission limit, correct functioning and regeneration of pollution control devices, crankcase emissions, on-board diagnostic systems, in-service performance of pollution control devices, durability, portable emission measurement system to verify in-use emissions, CO_2 and fuel consumption, measurement of engine power, reference fuels, and specific provisions to ensure correct operation of NO_x control measures. Implementation of these stringent emission standards is anticipated to cause a reduction in the fuel efficiency due to the exhaust emission control devices needed to meet emissions regulations for both NO_x and PM without the introduction of advanced combustion technologies.

Advanced combustion engine technologies being developed by the present authors are focused on

ICEs fuelled with gaseous fuels, operating in advanced combustion regimes, including modes of low-temperature combustion, which increase the efficiency beyond those of current advanced diesel engines and reduce engine-out emissions of NO_x and PM to near-zero levels. In addition to advanced combustion regimes, a reduction in the heat transfer, control of the load by the quantity of fuel injected, and a wide range of waste heat recovery technologies are also being considered to improve the engine efficiency further and to reduce the fuel consumption.

2 THE ALWAYS-LEAN-BURN DIRECT-INJECTION JET IGNITION ENGINE

The lean-burn direct-injection jet ignition (DI-JI) engine is an ICE developed to burn gaseous and liquid fuels more efficiently and completely within the cylinder of a four-stroke engine. This engine uses a fuel injection and mixture ignition system consisting of one main-chamber direct-injection (DI) fuel injector and one jet ignition (JI) pre-chamber per engine cylinder. The aim of the system is to increase the top brake efficiencies as well as to reduce the efficiency penalty changing the load for a diesel-like operation by the quantity of fuel injected enabled by the option to burn extremely lean fuel mixtures.

The small JI pre-chamber is connected to the main chamber through calibrated orifices and accommodates another DI fuel injector. In the spark plug version, the pre-chamber also accommodates a spark plug which ignites a pre-chamber mixture slightly richer than the bulk which, in turn, ignites the ultra-lean stratified main-chamber mixture through the multiple jets of hot reacting gases entering the in-cylinder volume [**7**].

Figure 1 presents a sectional view of the computer-aided design (CAD) model of the in-cylinder and JI pre-chamber volumes on the symmetry plane of a four-cylinder engine. The piston position is top dead centre (TDC). Details of the injectors towards the main-chamber and pre-chamber volumes are not included. The main-chamber injector is located at the centre of the combustion chamber close to the pre-chamber nozzles. A pressure sensor for combustion studies is also located in the centre. The pre-chamber injector is located on top of the pre-chamber close to the spark plug. The bowl in the piston is central to achieve a main-chamber fuel jet close to the pre-chamber nozzles. The JI pre-chamber has six nozzles. It is designed to fit a standard spark plug thread of diameter 14 mm. It accommodates one racing spark plug of diameter 10 mm [**8**]. Space is left to accommodate one pre-chamber injector. It features six equally spaced nozzles of diameter 1.25 mm. The pre-chamber volume is about 1.5 cm^3.

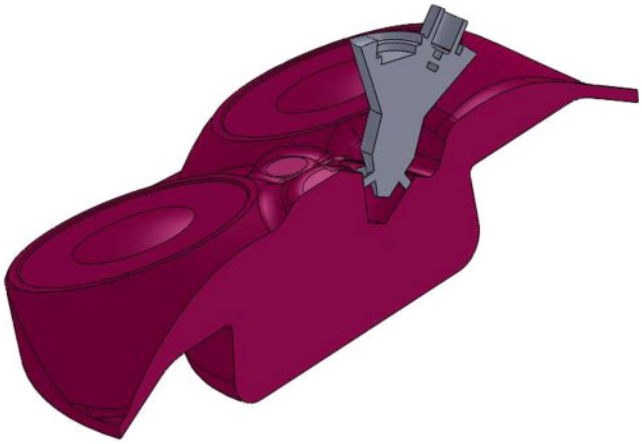

Fig. 1 Sectional view of the in-cylinder and pre-chamber volumes with the piston at the TDC position

The fuel injection and mixture ignition system operation is as follows. One fuel is injected directly within the cylinder by a main-chamber DI fuel injector operating one single injection or multiple injections to produce a lean stratified mixture preferably in the bulk. This inhomogeneous mixture is mildly lean in the inner region surrounded by air and some residuals from the previous cycle. The extension of the inner region may be reduced in size to achieve mean chamber-averaged mixtures ranging from slightly lean to extremely lean. Experiences so far have been realized with equivalent air-to-fuel ratios $\lambda = 1$ to $\lambda = 6.6$. This mixture is then ignited by one or more jets of the reacting gases that issue from the small pre-chamber connected to the main chamber via calibrated orifices, sourced from the same or an alternative fuel that is injected into it by a second DI fuel injector and then ignited by the spark plug discharge. Combustion starts slightly fuel rich in the very-small-volume pre-chamber and then moves very quickly to the main chamber through one or more nozzles, with one or more jets of hot reacting gases bulk igniting the main-chamber mixture. The jets of reacting gases enhance combustion of lean stratified mixtures within the main chamber through a combination of high thermal energy, multiple ignition points, and the presence of active radical species.

With reference to the homogeneous DI or PFI and the main-chamber spark ignition, inhomogeneous DI and JI offer the advantages of much faster, more complete, much leaner combustion, less sensitivity

to the mixture state and composition, and reduced heat losses to the main-chamber walls. This is because of the better fuel distribution for the same main-chamber-averaged fuel-to-air equivalence ratio lean conditions, the combustion in the bulk of the in-cylinder gases, the heat transfer cushion of air between hot reacting gases and walls, the availability of a very high ignition energy at multiple simultaneous ignition sites which ignite the bulk of the in-cylinder gases, and the start of main-chamber combustion aided by large concentrations of partially oxidized combustion products initiated in the pre-chamber which accelerate the oxidation of fresh reactants within the main chamber.

The advantages of the system are: a higher brake efficiency (the ratio of the engine brake power to the total fuel energy) and therefore a reduced brake specific fuel consumption (the ratio of the engine fuel flowrate to the brake power) for improved full-load operation of stationary and transport engines; efficient combustion of variable-quality fuel mixtures from near stoichiometry to extremely lean for load control (mostly throttleless) by the quantity of fuel injected for improved part-load operation of non-stationary engines; and the opportunity in the ultra-lean mode to produce near-zero NO_x in addition to the nearly zero PM with gaseous fuels.

JI and DI are potential enablers of higher-efficiency cleaner ICEs, where very lean mixtures of gaseous fuels could be burned with pollutants formation below Euro 6 levels, efficiencies approaching 50 per cent full load, and small efficiency penalties operating part load.

The concept of the coupling of the DI of the main-chamber fuel and bulk ignition by multiple jets of hot gases from a small pre-chamber fitted with a second fuel injector and a spark plug has been covered by many papers and patents, but only by researchers of Watson's group at the University of Melbourne and by the main author of this paper [**7**–**21**]. The concept is an original evolution of the idea of using jet-style ignition to enable the operation of a flame propagation engine with very lean mixtures explored many times, mostly in the large engine natural-gas industry; the marked differences in the DI fuel injector to the main chamber created mixtures from lean homogeneous to lean stratified in order to explore the many options of low-temperature combustion, and the small pre-chamber fitted with a second fuel injector and a spark plug enabled start of combustion by multiple jets of hot reacting gases originating from almost stoichiometric ignition of a small fraction of the total fuel.

The small size of the pre-chamber (1.5 cm^3 connected to a 1800 cm^3 displaced in-cylinder volume of the 11-l truck engine considered in the applications) is assumed to keep the amount of NO_x produced low, as otherwise this would be a major detriment of traditional pre-chamber engines even at very lean operating conditions. The spark plug life within the pre-chamber is generally not viewed as a major issue so long as cooling considerations are taken into account when designing the pre-chamber housing. However, the limited amount of space available to accommodate a spark plug and the therefore very far from optimal conditions may suggest replacement of a spark plug with a much smaller glow plug [**9**, **22**]. In the glow plug version of the ignition pre-chamber, the spark plug is replaced by a glow plug not only to increase durability and to reduce maintenance costs but also to increase packaging and to avoid the occurrence of locally fuel-rich conditions carefully controlling auto-ignition and pre-chamber injection. The operation of the glow plug pre-chamber is, on the other hand, much more complicated, and some additional studies are needed to develop the concept further. The DI-JI engine concept is therefore a novel idea, of particular relevance for gaseous fuels, and it definitely has potential for further interesting studies and developments.

3 SOME NOTES ON PRE-CHAMBER DESIGN AND INJECTOR SELECTION

If V_{PC} is the pre-chamber volume, V_{MCC} is the main-chamber combustion chamber volume, and V_D is the displaced volume ($V_D = \pi(B^2/4)S$, where B is the bore and S is the stroke), the true compression ratio is

$$CR = \frac{V_{PC} + V_{MCC} + V_D}{V_{PC} + V_{MCC}}$$

while the reference compression ratio is

$$CR^* = \frac{V_{MCC} + V_D}{V_{MCC}}$$

If η_V is the volumetric efficiency

$$\eta_V = \frac{m_a}{\rho_{a,i} V_D}$$

where m_a is the mass of air trapped within the cylinder when the intake valves are closed and $\rho_{a,i}$ is

the reference air density, then the mass of fuel to be injected within the pre-chamber is

$$m_{\mathrm{f,PC}} = \frac{(\mathrm{f/a})_{\mathrm{s}}}{\lambda_{\mathrm{PC}}} \eta_V \rho_{\mathrm{a,i}} (\mathrm{CR}-1) V_{\mathrm{PC}}$$

while the quantity of fuel to be injected within the main chamber is

$$m_{\mathrm{f,MC}} = \frac{(\mathrm{f/a})_{\mathrm{s}}}{\lambda_{\mathrm{MC}}} \eta_V \rho_{\mathrm{a,i}} [V_{\mathrm{D}} - (\mathrm{CR}-1) V_{\mathrm{PC}}]$$

where $(\mathrm{f/a})_{\mathrm{s}}$ is the stoichiometric fuel-to-air ratio (equal to 0.0642 for C_3H_8, 0.0584 for methane (CH_4), and 0.0294 for hydrogen (H_2)), λ_{PC} is the pre-chamber operational air-to-fuel equivalence ratio (slightly smaller than unity), and λ_{MC} is the main-chamber operational air-to-fuel equivalence ratio (much larger than unity; values of 2.5–6.6 cover the full-load range with negligible production of NO_x). η_V is approximately unity for naturally aspirated engines but can reach values up to 2.5 in highly turbocharged versions with a charge cooler, because of the recovery of the exhaust energy.

From previous relations, the main-chamber DI fuel injector has to deliver much larger quantities of fuel than the pre-chamber DI fuel injector does. The injection pressures required are 200–300 bar for the high-pressure (HP) main-chamber DI fuel injector, and 25–50 bar for the low-pressure (LP) pre-chamber DI fuel injector. In the case of the 1.5-l four-cylinder turbocharged engine, with volumetric efficiencies approaching $\eta_V = 2$, the amounts of C_3H_8 and CH_4 fuels introduced within the main chamber are about 24.5–12.25 mg and 22.5–11.25 mg respectively when running with $\lambda_{\mathrm{MC}} = 2.25$–4.5. Conversely, the amounts of fuel introduced within the pre-chamber are roughly 2.8 mg and 2.6 mg respectively with C_3H_8 and CH_4 fuels, i.e. 10–20 per cent of the main-chamber fuel.

Injectors are preferably of the multi-hole type and, if possible, operate with choked flow through nozzles. The isobaric properties of C_3H_8, CH_4, and H_2 at a pressure of 200 bar and temperatures of 300–400 K [**23**] show that C_3H_8 is a liquid at 300–370 K, with a density of 501–380 kg/m^3, and then supercritical [**23**], while CH_4 and H_2 are always supercritical with much lower densities of 155.3–98.5 kg/m^3 and 14.4–11.06 kg/m^3 respectively. The isobaric properties of C_3H_8, CH_4, and H_2 at a pressure of 50 bar and the same temperatures of 300–400 K show that C_3H_8 is a liquid at 300–370 K, with a density of 531–450 kg/m^3, and then supercritical [**23**], while CH_4 and H_2 are always supercritical with much lower densities of 35–24.6 kg/m^3 and 3.43–2.96 kg/m^3 respectively. Despite the fact that the speed of sound is higher in H_2 than in CH_4 and in C_3H_8 (equal to 1318.4 m/s for H_2, 449.5 m/s for CH_4, and 252.3 m/s for C_3H_8 in typical injection conditions), the mass flowrates are lower with H_2 than with CH_4 or C_3H_8, thus requiring larger flow passages.

Ideally, the main-chamber and pre-chamber injections should complete on approaching TDC, when the fast combustion process should start, initiated by the spark discharge. The fast-actuating HP high-flowrate main-chamber DI fuel injector must produce a bulk lean stratified mixture, fully jet controlled or mixed jet–wall controlled, and injection should occur with the valves closed. Because of the load control by the quantity of fuel injected, the injection times may vary considerably from lean $\lambda = 2.5$ to extremely lean $\lambda = 5$ and above. The LP low-flowrate pre-chamber DI fuel injector is in principle less demanding because it must introduce a smaller amount of fuel that does not change too much with load or speed without time constraints to produce slightly fuel-rich conditions within the small 1.5 cm^3 pre-chamber.

Prototype hardware has been defined so far using normal production injectors. However, better performances are possible by developing *ad hoc* solutions for both the main-chamber and the pre-chamber DI fuel injectors. Whereas one last-generation fast-actuating HP gasoline direct-injection (GDI) fuel injector could be used as the main-chamber injector for C_3H_8 for prototype applications where durability and dry-run capability are not an issue (e.g. one of the HP fast single-coil or piezo GDI injectors proposed in references [**24**] and [**25**]), a specific injector (e.g. the HP injector proposed in reference [**26**]) must be used for the short-injection-time, high-temperature, high-injection-pressure, high-durability, dry-run capability required with CH_4 and moreover with H_2.

The fast single-coil DI fuel injector reported in reference [**24**] provides (with gasoline fuel) flowrates up to 40 g/s at 200 bar, up to three multiple injections, hydraulic separation at multiple injections of not longer than 0.2 ms, and a hollow cone pattern with cone angles as required by the application. The double-acting multi-hole DI fuel injector used in the work in reference [**26**] has a much larger area, with an equivalent flow area of 0.7 mm^2 through 16 holes, and may deliver up to 20 g/s with C_3H_8 at 200 bar, with response times within 0.1 ms and a minimum injection duration of 0.5 ms. This latter injector has also been used with H_2 in prototype applications [**27**].

The size of the ignition pre-chamber is very small, just a few per cent of the combustion chamber volume at TDC and equal to about 1.5 cm^3. The JI pre-chamber is designed to be fitted within the traditional spark plug thread of diameter 14 mm to increase only marginally the level of complexity of designing a cylinder head with a JI pre-chamber replacing the standard main-chamber spark plug and to allow testing on the existing hardware. The 1–1.5 cm^3 volume and the operation with a slightly fuel-rich mixture are the values that have provided the best results so far [**15–21**]. A standard LP GDI injector (e.g. the LP injectors proposed in references [**25**] and [**28**]) can be used as the pre-chamber injector for prototype applications where again durability and dry-run capability are not issues with all the fuels. The jets of reacting gases from the ignition pre-chamber then ignite the main-chamber mixture. The diameters and number of nozzles control the flow of air (and residuals) from the main chamber to the pre-chamber during compression, and from the pre-chamber to the main chamber during the JI event, where the multiple jets of hot reacting products must enter the main chamber with sufficient speed and energy to ignite the main-chamber mixture. A configuration with six equally spaced nozzles of diameter 1.25 mm has provided so far the best results [**15–21**] igniting homogeneous lean main-chamber mixtures.

4 PREVIOUS EXPERIMENTAL AND LATEST COMPUTATIONAL RESULTS

Experimental results have been previously obtained on a single-cylinder optical access test engine [**19**]. The engine was naturally aspirated, with a four-valve cylinder head and a pent-roof combustion chamber, and accommodates a central hydrogen-assisted jet ignition (HAJI) pre-chamber, plus one side direct injector and one port injector to simulate the DI operation and the port fuel injection (PFI) operation respectively, and also a pressure sensor for combustion data analysis. The engine had a large bore-to-stroke ratio (having a bore of 89 mm and a stroke of just 66 mm) and a CR of 10.3:1 and was not cooled. Early and late DIs were considered for lean stratified operation. The JI device had six holes of diameter 1.25 mm and a volume of 1.3 cm^3 and accommodated a fuel injector for H_2 and a small spark plug of diameter 8 mm. The mixture preparation was not optimal, because of the side location of the injector and the poor atomization properties of the injector, as well as the low temperatures of the in-cylinder walls and in-cylinder charge. Experiments were carried out with C_4H_{10} as the main-chamber fuel and H_2 as the JI pre-chamber fuel. When the amount of H_2 injected in the JI pre-chamber is about 2 mg/s (roughly 5 per cent of the total fuel energy), the amount of C_4H_{10} is 0.11 g/s, and the engine is running at 1500 r/min with λ controlled by throttling the intake; the combustion durations $\Delta\theta_{5-95\%}$ were 17–19° crank angle with $\lambda = 1.2$–1.4 and early DI, and 17–20° crank angle with $\lambda = 1.6$–2.0 and late DI [**19**]. Further experimental data are presented in the Appendix.

Computations have been performed using computational fluid dynamics (CFD) and computer-aided engineering (CAE) tools. A CFD tool is used to simulate the detailed fluid dynamics and combustion of the stand-alone pre-chamber in three dimensions, while a CAE tool is used to describe the full cyclic engine operation including the in-cylinder and pre-chamber processes. CFD simulations are performed using STAR-CCM [**32**], while CAE simulations are performed using GT-POWER [**30**] and WAVE [**31**]. GT-POWER and WAVE are the industry-standard CAE engine simulation tools, used by most leading engine and vehicle makers and their suppliers. STAR-CCM [**32**] is one of the most promising CFD platforms delivering the entire CFD process from CAD to post-processing in a single integrated software environment. Innovations such as built-in surface wrapping and advanced automated meshing have quickly established for STAR-CCM a reputation for producing high-quality results in a single code with minimum user effort. STAR-CCM features automatic meshing technology and a comprehensive selection of physics models delivering accurate solutions in an easy-to-use environment.

STAR-CCM simulations of combustion evolution have been performed for the stand-alone pre-chamber connected to a simplified main chamber where constant-pressure boundary conditions can apply. Figure 2 presents a sectional view of the CAD model of the ignition pre-chamber with a multi-hole fuel injector fitted. The spark plug is located top right, while the LP injector is located top left. The actual LP injector is replaced by a volume connected to the pre-chamber through multiple nozzles. The actual sac volume and the diameter and length of nozzles are much smaller than those represented. An inlet velocity boundary condition is used at the top of the injection volume, while a pressure outlet condition is used along the spherical surface, and all the other boundaries are adiabatic solid walls.

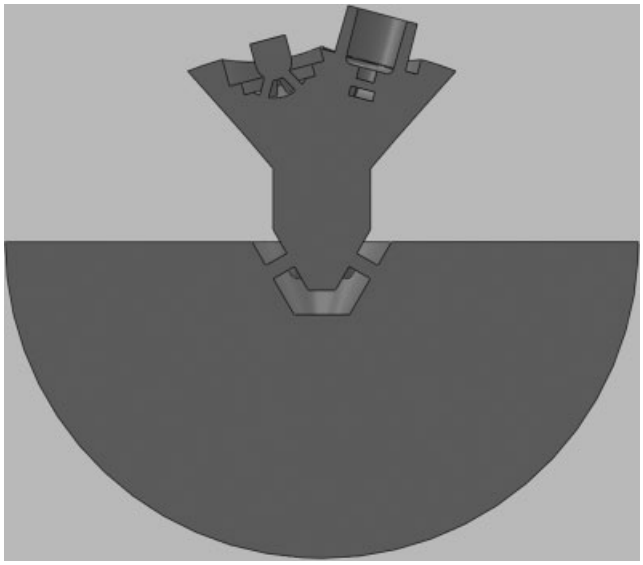

Fig. 2 Sectional view of the ignition pre-chamber connected to a downstream hemisphere

Ignition is started after injecting a slightly rich mixture of fuel within the pre-chamber. Initial conditions within the pre-chamber are high temperatures and pressures typical of engine operation at TDC. The initial composition of the fluid within the domain is just air (no fuel downstream of the pre-chamber). The effect of a variable in-cylinder volume downstream which produces a very intense flow from the main chamber to the pre-chamber through the connecting nozzles is neglected. The main goal of these computations is to determine how long it takes from spark discharge combustion initiation within the pre-chamber to obtain multiple jets of hot reacting products which ignite the main-chamber mixture. The mean and turbulent velocity fields within the pre-chamber are underestimated, and therefore the turbulent transport and diffusion are also underestimated.

The flow is considered to be turbulent, compressible, and reacting, and to contain multiple species. Turbulence is modelled using a $k-\varepsilon$ model with a two-layer all $y+$ wall treatment [**32**]. Combustion is represented through a three-step eddy break-up (EBU) [**32**] for C_3H_8 and CH_4 and a one-step EBU for H_2. For C_3H_8 combustion, the reactions are

$$C_3H_8 + 1.5O_2 \rightarrow 3CO + 4H_2$$

$$CO + 0.5O_2 \rightarrow CO_2$$

$$H_2 + 0.5O_2 \rightarrow H_2O$$

while, for CH_4 combustion, the first reaction to CO and H_2 is different, producing the kinetics

$$CH_4 + 0.5O_2 \rightarrow CO + 2H_2$$

$$CO + 0.5O_2 \rightarrow CO_2$$

$$H_2 + 0.5O_2 \rightarrow H_2O$$

Ignition is started in the computational cells included in a small spherical volume in between the spark plug electrodes, where the fuel is prescribed to burn within a given time interval. After that, the EBU model computes the evolution of combustion from the concentrations of the reactants and products and the turbulence mixing time [**32**] according to

$$R_F = -\frac{\rho}{M_F}\frac{1}{\tau_{mix}} A_{EBU} \min\left[Y_F, \frac{Y_O}{s_O}, B_{EBU}\left(\frac{Y_{P_1}}{s_{P_1}} + \cdots + \frac{Y_{P_j}}{s_{P_j}}\right)\right]$$

where $\tau_R = \tau_{mix}$ and $\tau_{mix} = K/\varepsilon$, with K the turbulent kinetic energy and ε its dissipation rate. Two EBU coefficients are used for each equation. Standard values $A_{EBU} = 4$ and $B_{EBU} = 0.5$ are used for the EBU coefficients.

The previous expression does not account for the chemical kinetics that may be relevant during ignition and describe the flame behaviour close to solid boundaries where, because the turbulent mixing timescale τ_{mix} decreases with decreasing distance from solid surfaces, the reaction rates are overpredicted in near-wall regions. The hybrid kinetics–EBU model [**32**] accounts for finite rate effects by assuming that the actual reaction rate is the minimum from kinetics- and turbulent-mixing-controlled reactions. The mixing timescale τ_R in the previous equation is then augmented by a timescale derived from the chemical reaction rate τ_{kin} for finite rate kinetics to avoid the near-wall misrepresentation of flames. The combined timescale model [**32**] then assumes that $\tau_R = \tau_{mix} + \tau_{kin}$, where τ_{kin} is computed from the kinetics model.

The computational grid is made up of just 100 000 polyhedral cells to keep the computational time and the internal memory requirements very low, below 400 000 kB memory usage. Figures 3 to 6 present the results of computations for C_3H_8 0.1 ms after start of combustion. Figure 3 presents the computed temperature field, while Figs 4 and 5 present the computed field of the combustion products H_2O and CO_2 and finally Fig. 6 presents the velocity field. After 0.1 ms from the spark, hot products of combustion are travelling at a high speed through the main chamber. In the case of operation with the pre-chamber fitted on a cylinder head, these multiple jets would ignite the lean stratified mixture in the

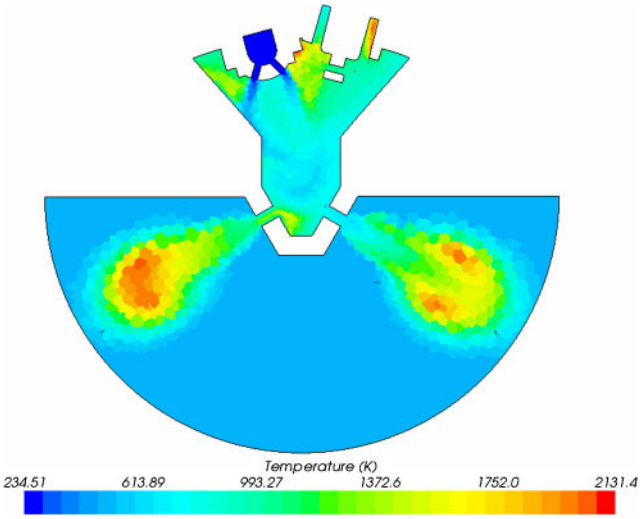

Fig. 3 Temperature field 0.1 ms after the start of combustion (C_3H_8)

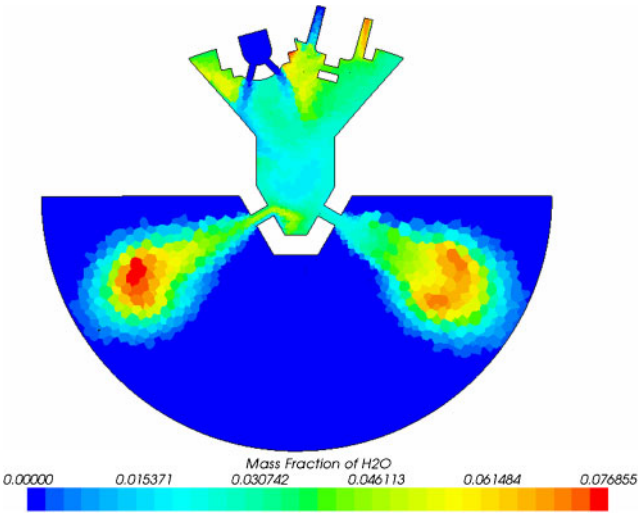

Fig. 4 H_2O field 0.1 ms after the start of combustion (C_3H_8)

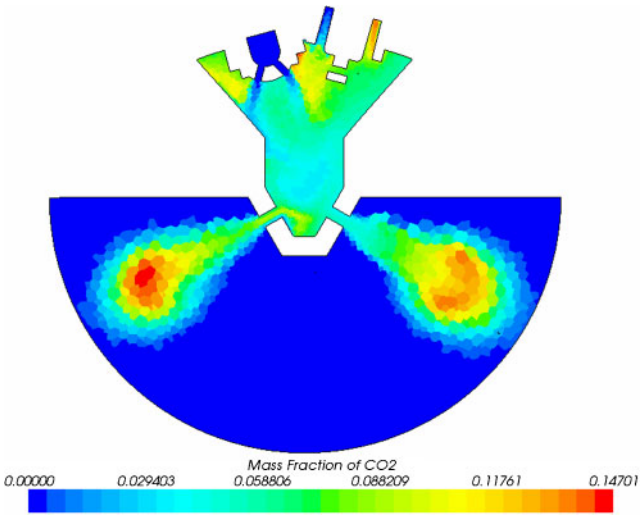

Fig. 5 CO_2 field 0.1 ms after the start of combustion (C_3H_8)

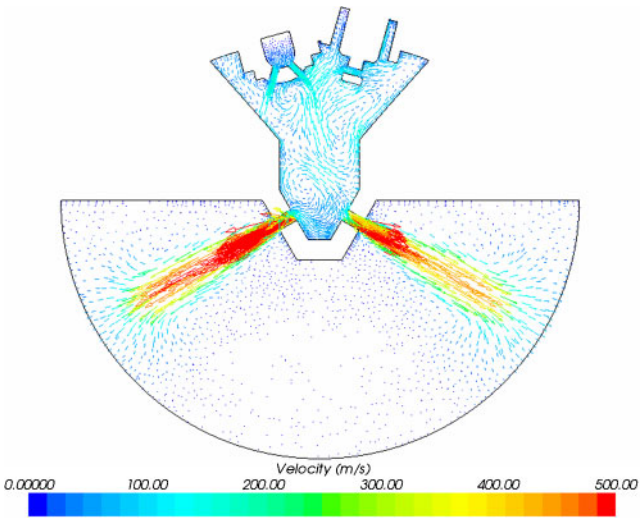

Fig. 6 Velocity field 0.1 ms after the start of combustion (C_3H_8)

bulk of the in-cylinder volume passing through regions with very little fuel available.

With CH_4, the combustion kinetics are slower than with C_3H_8, while the combustion kinetics are faster with H_2. As previously stated, within the engine, because of the much larger turbulent field and the enhanced mixing of the downward-injected fluid with the upward airflow from the main chamber, the heat transfer from the hot walls is expected to reduce the time frame of the pre-chamber ignition phenomena further.

These CFD simulations of the stand-alone pre-chamber have been performed with CH_4, C_3H_8, and H_2 fuel to estimate the delay between the start of combustion within the pre-chamber and sufficient penetration of the hot, partially burned reacting gases within the main chamber. Delay times are longer with CH_4 and shorter with H_2 because of the different kinetics. As a general statement, it may be assumed that these times are of the order of 0.1 ms. The computed delay times will then be used as an input for the CAE simulations of the full engine.

CFD simulations of the stand-alone pre-chamber may help to define the pre-chamber geometry, especially with respect to the diameter, number, and orientation of the nozzles connecting the main chamber to the pre-chamber, as well as to the definition of the injector nozzles, including the sac volume and diameter, and the number and orientation of the nozzles. Mainly because of the neglected

in-flow from the main chamber, these simulations are much less effective than CFD simulations of flow within the pre-chamber plus in-cylinder covering compression and expansion strokes. However, these latter simulations, although incontestably more helpful, are undoubtedly also more expensive, with major problems because of the different spatial resolution scales to be used within the injector, the pre-chamber, and the main chamber. (In the truck engine application discussed later, the displaced volume of a single cylinder is 1800 cm^3, the pre-chamber volume is 1–1.5 cm^3, the diameters of the multi-hole injector nozzles are of the order of 10^{-4} m, and the lifts of injector needle are of the order of 10^{-5} m.) Therefore, stand-alone pre-chamber, pre-chamber-plus-in-cylinder, and CAE engine simulations as well as the analogous experiments should all be considered in the development of the DI-JI engine concept.

Full-cycle engine simulations have then been performed using GT-POWER [**30**]. In these computations, the ignition pre-chambers are fitted on the cylinder head of a small, high-technology, 1.5-l, four-cylinder, highly turbocharged engine having V_D = 375 cm^3, V_{PC} = 1.5 cm^3, a CR of 13.8, and a CR* of 14.5 which have been better described in references [**8**] and [**10**] to [**14**]. With reference to the model previously described in these references, the pre-chamber is now modelled as a volume connected through the main chamber through orifices where fluid can be injected and chemical reactions can occur. All the HP and LP rails are modelled, as well the HP and LP injectors. These injectors are modelled as volumes connected to the main chamber (HP DI injector) and the pre-chamber (LP DI injector) respectively through orifices and connected to their feeding rail through a passage area prescribed in time. A very basic one-step reaction is considered for combustion within the pre-chamber. Following ignition, all the reactants are replaced by the hot products within a given burning time. This burning time is the value resulting from the previous CFD simulations. In reality, combustion within the pre-chamber is only incomplete, and partially burned products are also injected in the main chamber. These differences are, however, negligible in the description of flow towards and from the pre-chamber of concern here.

The results are presented in Figs 7 to 9 for operation of the engine with C_3H_8 and $\lambda = 2.25$, running at 7500 r/min. The flow from the sac volume of the HP injector to the main chamber is choked shortly after injection starts. The flow from the sac volume of the LP injector to the pre-chamber is also choked shortly after injection starts. Figure 7 shows the pressure drop across the nozzles from the pre-chamber to the main chamber, while Figs 8 and 9 show the velocity and the Mach number respectively through one of the six nozzles connecting the pre-chamber to the main chamber. Each nozzle diameter is 1.25 mm, while the flow coefficient is 0.85 for a total effective area of 2 mm^2. During the compression stroke, the pressure in the main chamber is

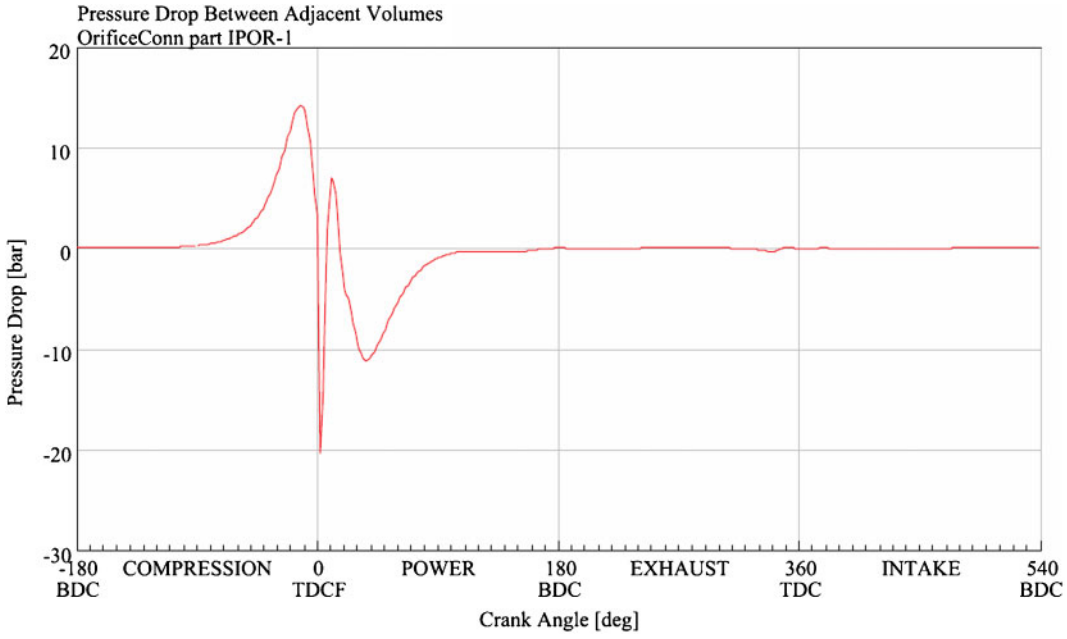

Fig. 7 Pressure drop across the pre-chamber to the main-chamber nozzles (C_3H_8) (BDC, bottom dead centre; TDC, top dead centre)

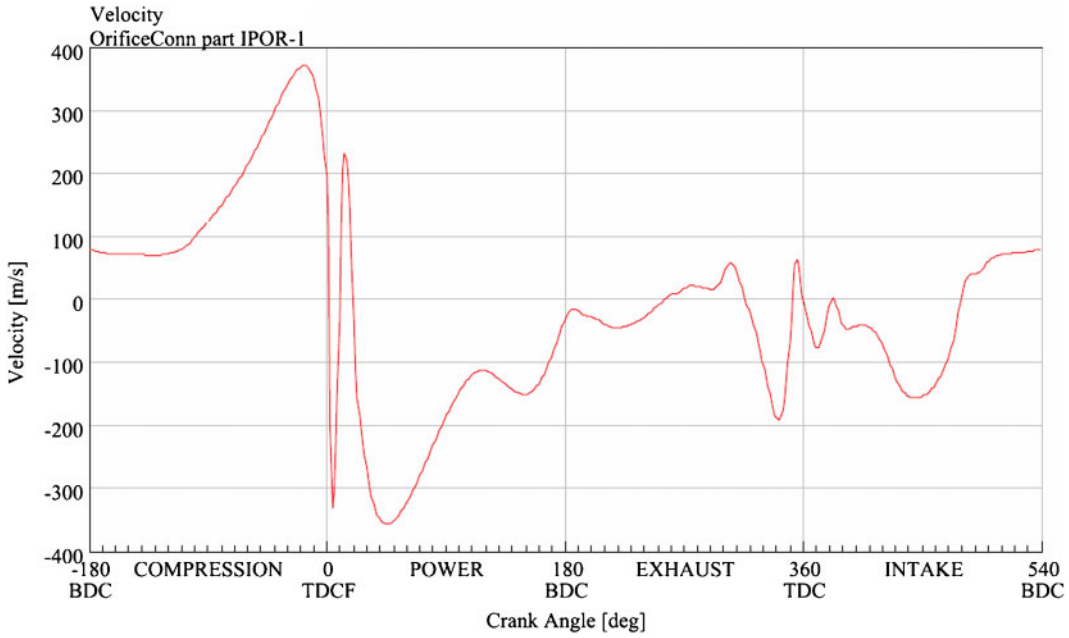

Fig. 8 Velocity through the pre-chamber to the main-chamber nozzles (C_3H_8) (BDC, bottom dead centre; TDC, top dead centre)

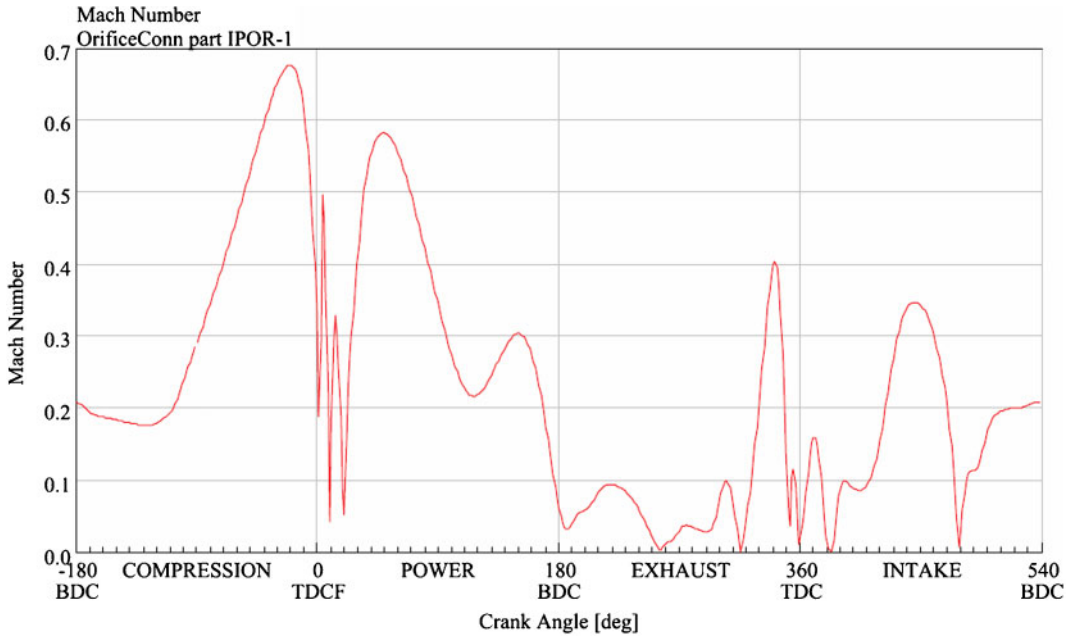

Fig. 9 Mach number through the pre-chamber to the main-chamber nozzles (C_3H_8) (BDC, bottom dead centre; TDC, top dead centre)

higher than the pressure in the pre-chamber, and the flow of air and residuals is moving from the main chamber to the pre-chamber. Towards the end of the compression stroke, injection occurs within the main chamber and the pre-chamber. Firing is placed at TDC, when both the pre-chamber and the main-chamber injections end. The addition of hot products into the pre-chamber produces a higher pressure in the pre-chamber than in the main chamber. The flow from the pre-chamber to the main chamber lowers the pressure within the pre-chamber. Combustion finally starts in the main chamber. As soon as the combustion in the main chamber proceeds, the pressure in the main chamber again becomes higher than the pressure in the pre-chamber and the flow again is from the main

chamber to the pre-chamber. The combustion duration $\Delta\theta_{10–90\%}$ is assumed to be about 10° crank angle with C_3H_8. During the power stroke, the effect of the increased volume due to the piston motion slightly exceeds the effect of the heat release, the pressure within the main chamber falls below the pre-chamber pressure, and the flow is again from the pre-chamber to the main chamber up to the end of the power stroke. The quantity of unburned fuel trapped within the pre-chamber is negligible. These results clearly show the relevance of the neglected flow from and to the main chamber that will certainly deserve better consideration if the JI pre-chamber has to be optimized.

STAR-CCM [**32**] injection and combustion simulations have been performed for a single engine cylinder of a larger 3.6-l, naturally aspirated six-cylinder gasoline engine fuelled with H_2. This engine has $V_D = 600\,\text{cm}^3$, $V_{PC} = 1.5\,\text{cm}^3$, a CR of 10.8, and a CR* of 11.0. Computations start when the intake valve closes, where the initial conditions are set by using the results of the CAE simulations, and end when the exhaust valve opens. The piston moves following the compression and expansion strokes, and the computational domain made up of the in-cylinder volume contracts or expands accordingly. The computational grid is made up of 300 000 polyhedral cells to keep the computational time and the internal memory requirements below 1 600 000 kB memory usage. Morphing is used to change the grid density to the variable in cylinder space, aiming to produce computationally effective mesh elements in size and shape. The main-chamber and pre-chamber injections are performed with very basic single-hole injectors where the sonic velocity is set during the injector opening times. The spark discharge is simulated as a pulse temperature igniter, i.e. a small sphere in between the electrodes where the temperature rises to 2500 K during a prescribed time. Simulations have been performed neglecting the residual gases within the cylinder and the pre-chamber at intake valve closure.

The flow is considered turbulent, compressible, and reacting and contains multiple species. Turbulence is modelled using a Reynolds-averaged Navier–Stokes (RANS) turbulence model, in particular, the two-equation $k-\varepsilon$ model with a two-layer all $y+$ wall treatment [**32**]. Other modelling of turbulence is available, including a large-eddy simulation and a detached-eddy simulation, and within the RANS family the Spalart–Allmaras, $k-\Omega$, or Reynolds stress transport variants; however, the $k-\varepsilon$ RANS is preferred for simplicity, generality, and reliability. Kinetics equations are obtained by using DARS-CFD [**33**]. The kinetics equations are presented in Table 1. A, n, and E_a are the Arrhenius rate constants given by

$$k = AT^n\, e^{-E_a/(RT)}$$

The transport and diffusion equations are solved for the nine chemical species, namely for O_2, H_2, H_2O, H, O, OH, HO_2, and H_2O_2. STAR-CCM solves the partial differential equations for energy and species conservation [**32**] given by

$$\frac{\partial}{\partial t}\rho Y_k + \frac{\partial}{\partial x_j}\left(\rho u_j Y_k + F_{k,j}\right) = 0$$

$$\frac{\partial}{\partial t}\rho h + \frac{\partial}{\partial x_j}\left(\rho u_j h + F_{h,j}\right) = \frac{\partial}{\partial t}p + u_j\frac{\partial}{\partial x_j}p + \tau_{i,j}\frac{\partial}{\partial x_j}u_i$$

while DARS-CFD solves the ordinary differential equations for chemical kinetics [**33**] given by

$$\frac{\partial}{\partial t}Y_i = \frac{\omega_i W_i}{\rho}$$

When the chemical kinetics are the limiting factor of the reacting system under investigation, near-perfect mixing of reactants and products is usually accomplished. However, normally these mixing mechanisms have to rely on fluid motion or large-scale eddies and turbulence to provide the mixing. Local turbulence is particularly important as it promotes micro-scale mixing among the gas species. If the turbulence is too weak to provide fast mixing among the gas species, the micromixing process will interfere with the chemical kinetics. The turbulence intensity is assumed to affect the combustion scaling reaction rates using the Kong–Reitz model [**34**] according to

$$s_i^t = s_i^l \frac{\tau_{kin}}{\tau_{kin} + f\tau_{turb}}$$

where

$$\tau_{turb} = C\frac{K}{\varepsilon}$$

and

$$f = \frac{1-\exp(-r)}{0.632}$$

$$r = \frac{m_{H_2O} + m_{H_2}}{1 - m_{N_2}}$$

Figures 10 to 15 present the temperature fields within the in-cylinder volume at different crank

Table 1 DARS preprocessor H_2–O_2 kinetic mechanism (the units are cm^3 mol s cal K)

Reaction		Arrhenius parameters		
		A	N	E_a
r1f	$H_2+O_2=2OH$	1.700×10^{13}	0.000	1.999×10^{2}
r1b	$H_2+O_2=2OH$	2.223×10^{10}	3.877×10^{-1}	1.202×10^{2}
r2f	$H_2+OH=H_2O+H$	1.170×10^{9}	1.300	1.517×10
r2b	$H_2+OH=H_2O+H$	7.980×10^{10}	9.726×10^{-1}	8.200×10
r3f	$H+O_2=OH+O$	2.000×10^{14}	0.000	7.029×10
r3b	$H+O_2=OH+O$	6.712×10^{11}	3.742×10^{-1}	-1.190
r4f	$O+H_2=OH+H$	1.800×10^{10}	1.000	3.693×10
r4b	$O+H_2=OH+H$	7.014×10^{9}	1.014	2.866×10
r5f	$H+O_2+M_1=HO_2+M_1$	2.100×10^{18}	-1.000	0.000
r5b	$H+O_2+M_1=HO_2+M_1$	6.276×10^{20}	-1.660	2.142×10^{2}
r6f	$H+2O_2=HO_2+O_2$	6.700×10^{19}	-1.420	0.000
r6b	$H+2O_2=HO_2+O_2$	2.002×10^{22}	-2.080	2.142×10^{2}
r7f	$H+O_2+N_2=HO_2+N_2$	6.700×10^{19}	-1.420	0.000
r7b	$H+O_2+N_2=HO_2+N_2$	2.002×10^{22}	-2.080	2.142×10^{2}
r8f	$OH+HO_2=H_2O+O_2$	5.000×10^{13}	0.000	4.184
r8b	$OH+HO_2=H_2O+O_2$	4.033×10^{14}	7.798×10^{-2}	2.972×10^{2}
r9f	$H+HO_2={}_2OH$	2.500×10^{14}	0.000	7.950
r9b	$H+HO_2={}_2OH$	3.867×10^{10}	7.930×10^{-1}	1.544×10^{2}
r10f	$O+HO_2=O_2+OH$	4.800×10^{13}	0.000	4.184
r10b	$O+HO_2=O_2+OH$	2.212×10^{12}	4.189×10^{-1}	2.221×10^{2}
r11f	$2OH=O+H_2O$	6.000×10^{8}	1.300	0.000
r11b	$2OH=O+H_2O$	1.050×10^{11}	9.591×10^{-1}	7.510×10
r12f	$H_2+M_2=2H+M_2$	2.230×10^{12}	5.000×10^{-1}	3.874×10^{2}
r12b	$H_2+M_2=2H+M_2$	6.310×10^{10}	7.542×10^{-1}	-5.301×10
r13f	$O_2+M=2O+M$	1.850×10^{11}	5.000×10^{-1}	3.998×10^{2}
r13b	$O_2+M=2O+M$	4.508×10^{7}	1.115	-1.038×10^{2}
r14f	$H+OH+M_3=H_2O+M_3$	7.500×10^{23}	-2.600	0.000×10
r14b	$H+OH+M_3=H_2O+M_3$	1.808×10^{27}	-3.182	5.073×10^{2}
r15f	$H+HO_2=H_2+O_2$	2.500×10^{13}	0.000	2.929×10
r15b	$H+HO_2=H_2+O_2$	2.956×10^{12}	4.053×10^{-1}	2.292×10^{2}
r16f	$2HO_2=H_2O_2+O_2$	2.000×10^{12}	0.000	0.000
r16b	$2HO_2=H_2O_2+O_2$	5.131×10^{13}	-1.776×10^{-1}	1.553×10^{2}
r17f	$H_2O_2+M=2OH+M$	1.300×10^{17}	0.000	1.904×10^{2}
r17b	$H_2O_2+M=2OH+M$	2.622×10^{9}	1.630	-3.268×10
r18f	$H_2O_2+H=HO_2+H_2$	1.600×10^{12}	0.000	1.590×10
r18b	$H_2O_2+H=HO_2+H_2$	7.375×10^{9}	5.829×10^{-1}	8.682×10
r19f	$H_2O_2+OH=H_2O+HO_2$	1.000×10^{13}	0.000	7.531
r19b	$H_2O_2+OH=H_2O+HO_2$	3.144×10^{12}	2.556×10^{-1}	1.453×10^{2}

angle positions about the firing TDC. The engine speed is 7500 r/min, while the air-to-fuel equivalent ratio of the H_2-fuelled engine is $\lambda = 2.25$. The spark is advanced with reference to the TDC position to allow combustion initiation. The kinetics are important in the early phase of combustion, and ignition of the pre-chamber mixtures takes a finite time despite the almost-stoichiometric conditions. As soon as combustion within the pre-chamber is fully initiated, it does not need much to obtain a jet of partially combusted hot products which spread combustion all over the main chamber, where combustion then completes within a short time despite the lean composition.

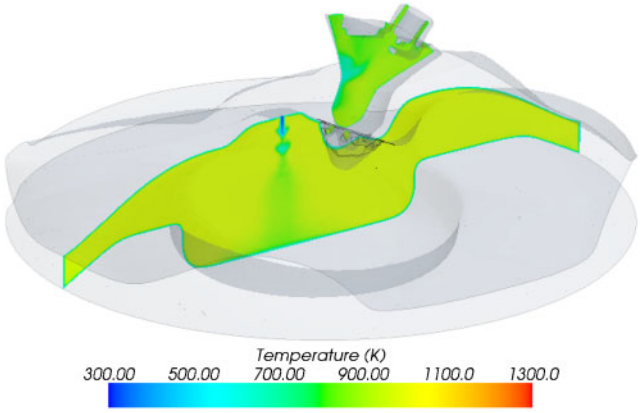

Fig. 10 Computed temperature fields within the cylinder 20° crank angle before top dead centre (BTDC) (H_2)

Combustion duration $\Delta\theta_{10\text{–}90\%}$ is less than 10° crank angle with H_2. Despite the fact that both the modelling of the flows through the pre-chambers and the interaction with the fuel jets is demanding, and modelling the heat transfer and combustion is a significant challenge even for computational tools of well-tested capabilities, predictions provide a combustion duration in line with the past measurements reported in reference [**19**], where combustion durations $\Delta\theta_{5\text{–}95\%}$ of about 17° crank angle were obtained for C_4H_{10} even with the poor mixture preparation

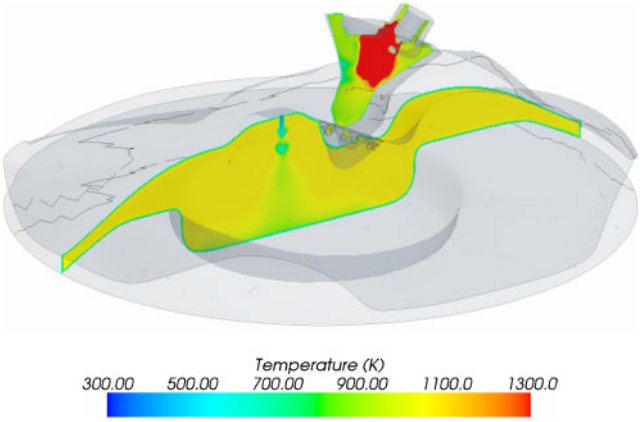

Fig. 11 Computed temperature fields within the cylinder 10° crank angle BTDC (H_2)

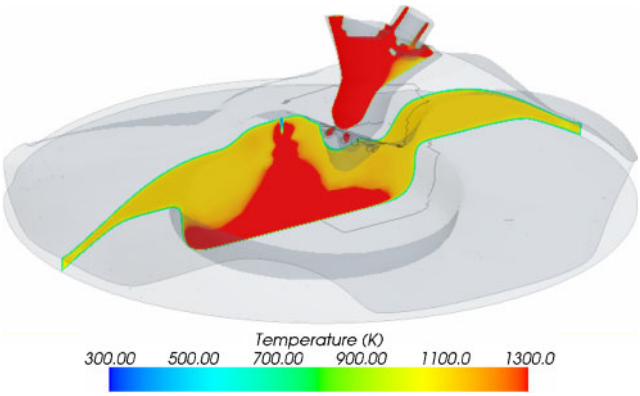

Fig. 12 Computed temperature fields within the cylinder at TDC (H_2)

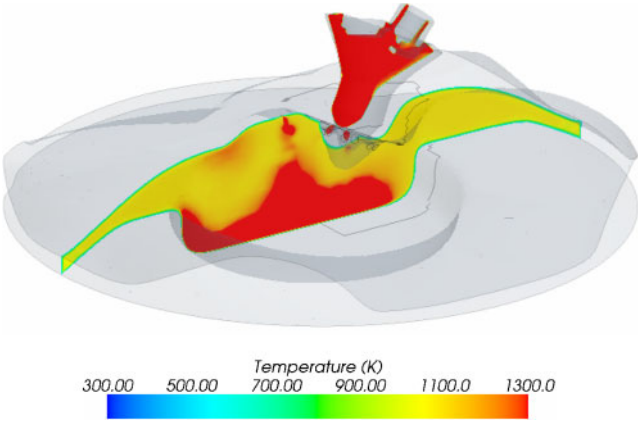

Fig. 13 Computed temperature fields within the cylinder 10° crank angle after top dead centre (ATDC) (H_2)

because of the side injector of poor atomization properties and the low temperatures of the in-cylinder walls and charge. The latest modelling

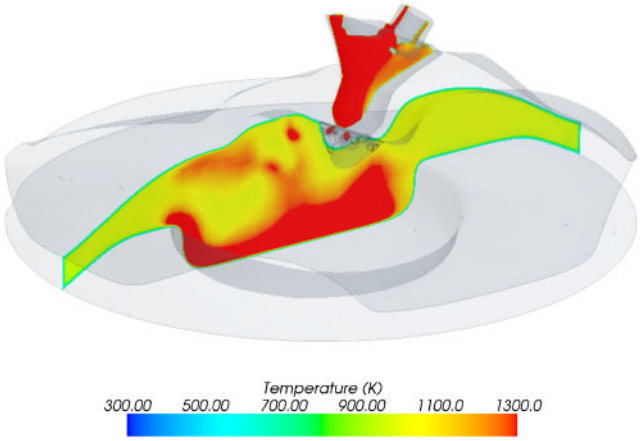

Fig. 14 Computed temperature fields within the cylinder 20° crank angle ATDC (H_2)

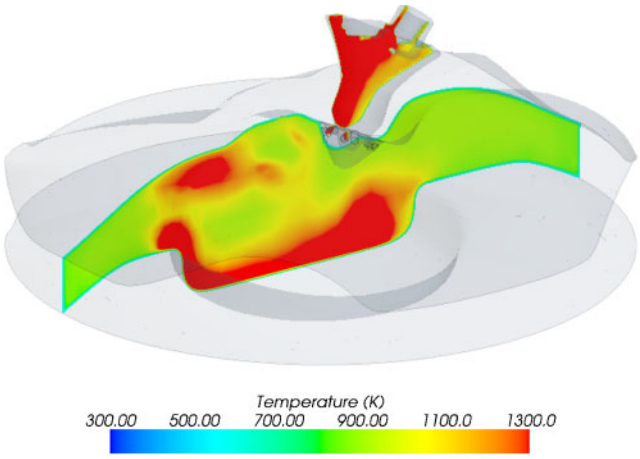

Fig. 15 Computed temperature fields within the cylinder 30° crank angle ATDC (H_2)

activity provides a novel detailed description of the phenomena governing the pre-chamber and main-chamber mixture formation and combustion evolution, providing both a better understanding of the potentials of DI coupled to JI to achieve very fast combustion rates in the case of mixtures that are also very lean (only conjectured in previous experiments [**19**]) and something that is worth sharing with the wider community. The computed fast rate of combustion of the DI-JI engine concept is also in line with the other experiments performed on different pre-chamber and main-chamber geometries in the case of PFI and homogeneous charge [**15–21**]. The computed fast rate of combustion of the DI-JI engine concept has therefore to be considered reliable. This fast rate of combustion with almost all the λ value is of particular significance for achieving very high top full-load and part-load brake efficiencies starting the main-chamber

heat release process about TDC and completing the process shortly afterwards.

GT-POWER [**30**] results obtained on the small, high-technology, 1.5-l, four-cylinder, highly turbocharged engine fuelled with C_3H_8 and H_2 [**13**] and having $V_D = 375\,cm^3$, $V_{PC} = 1.5\,cm^3$, a CR of 13.8 and a CR* of 14.5 show very interesting brake specific fuel consumption (BSFC) and brake efficiency results. In the engine speed range 3500–7500 r/min, the BSFC at wide-open throttle and maximum brake torque or knock-limited spark timing has a minimum of 165 g/kW h with C_3H_8 and less than 65 g/kW h with H_2 at about 3500 r/min, corresponding to brake efficiencies of almost 48 per cent. These results clearly show the potentials to achieve even better brake efficiencies exceeding the 50 per cent mark in the engine redesigned for lower speeds, where friction losses are lower and air-to-fuel equivalence ratios may be even leaner.

WAVE simulations [**31**] have been finally performed for a production 11-l, in-line, six-cylinder, 24-valve diesel truck engine modified to fit a JI pre-chamber and to run C_3H_8 fuel. The baseline diesel truck engine is turbo charged, with an intercooler and cooled exhaust gas recirculation, a full-load boost of 1.5–2.6, a bore B of 123 mm, a stroke S of 152 mm, a displaced volume V_D per cylinder of 1806 cm^3, a connecting-rod length L of 255 mm, and a compression ratio CR* of 16; it operates full load with $\lambda = 1.55$. The LPG version is obtained by replacing the diesel fuel injector with a DI fuel injector for the LPG fuel plus a JI pre-chamber, and reducing the compression ratio CR to 12. Operation with $\lambda = 1.55$ provides similar performances to the diesel engine and it is considered first. The brake thermal efficiency, brake mean effective pressure (BMEP), and brake specific CO_2 production are presented in Figs 16, 17, and 18 respectively for the diesel and LPG versions.

Average CO_2 emissions from the HC fuels are computed considering an oxidation factor to be applied to the carbon content to account for the small portion of the fuel that is not oxidized into

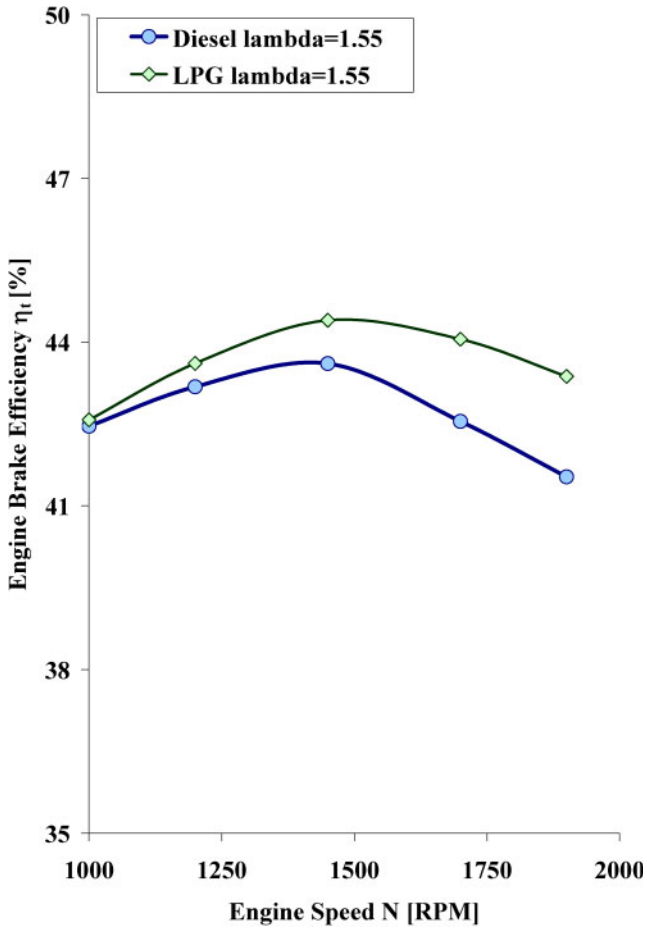

Fig. 16 Computed brake efficiency for the diesel- and the LPG-fuelled truck engine with $\lambda = 1.55$

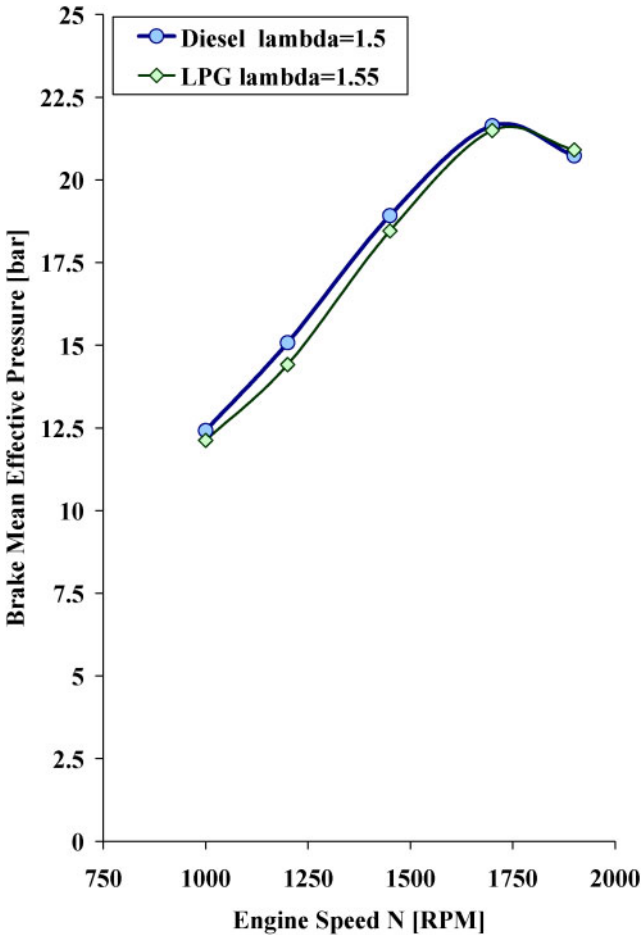

Fig. 17 Computed BMEP for the diesel- and the LPG-fuelled truck engine with $\lambda = 1.55$

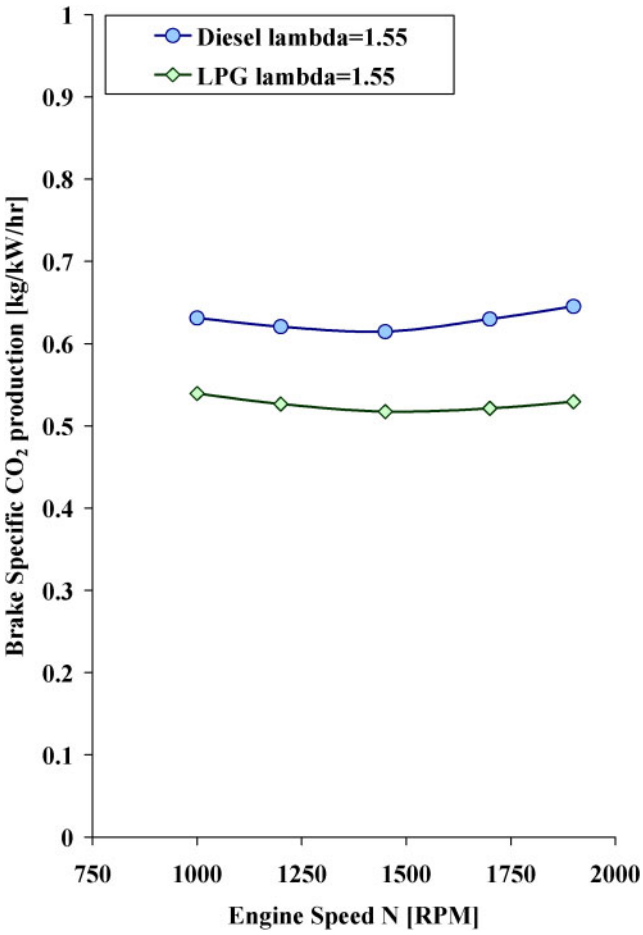

Fig. 18 Computed brake specific CO_2 production for the diesel- and the LPG-fuelled truck engine with $\lambda = 1.55$

CO_2. The Intergovernmental Panel on Climate Change guidelines for calculating emissions inventories requires that an oxidation factor be applied to the carbon content to account for the small portion of the fuel that is not oxidized into CO_2. For all oil and oil products, the oxidation factor used is 0.99 (99 per cent of the carbon in the fuel is eventually oxidized, while 1 per cent remains unoxidized). Finally, to calculate the CO_2 emissions from 1 kg of fuel, the carbon emissions are first obtained from the ratio of the molecular weight of carbon to the molecular weight of the HC fuel, and then the carbon emissions are multiplied by the ratio of the molecular weight of CO_2 to the molecular weight of carbon. Diesel fuel is considered an HC fuel having the formula $C_{15}H_{25.05}$ and a lower heating value (LHV) of 4.28×10^7 J/kg. LPG fuel is considered to have the formula C_3H_8 and an LHV of 4.655×10^7 J/kg. The number of kilograms of CO_2 per kilogram of C_nH_m fuel is 3.19 for diesel, 3.13 for gasoline, 2.97 for C_3H_8, and 2.72 for CH_4.

The LPG converted engine has approximately the same performance as the diesel engine running at about the same air-to-fuel equivalence ratio (i.e. the same BMEP versus the engine speed full load). This feature makes the conversion extremely attractive, because most of the vehicle management system can remain unaltered. The LPG converted engine has clear advantages in terms of CO_2 production, showing an almost 20 per cent reduction, and an increased efficiency of up to 2 per cent at higher speeds because spark-plug-initiated JI combustion is less sensitive to the engine speed than is diffusion combustion. The major advantage of LPG is, however, the negligible PM production because the partially premixed gaseous combustion replaces the liquid diffusion combustion of diesel requiring no after-treatment to meet Euro 6 emission standards. NO_x formation within the LPG engine is expected to require after-treatment to meet Euro 6 emission standards when running these air-to-fuel equivalence ratios. Figures 19 and 20 finally present

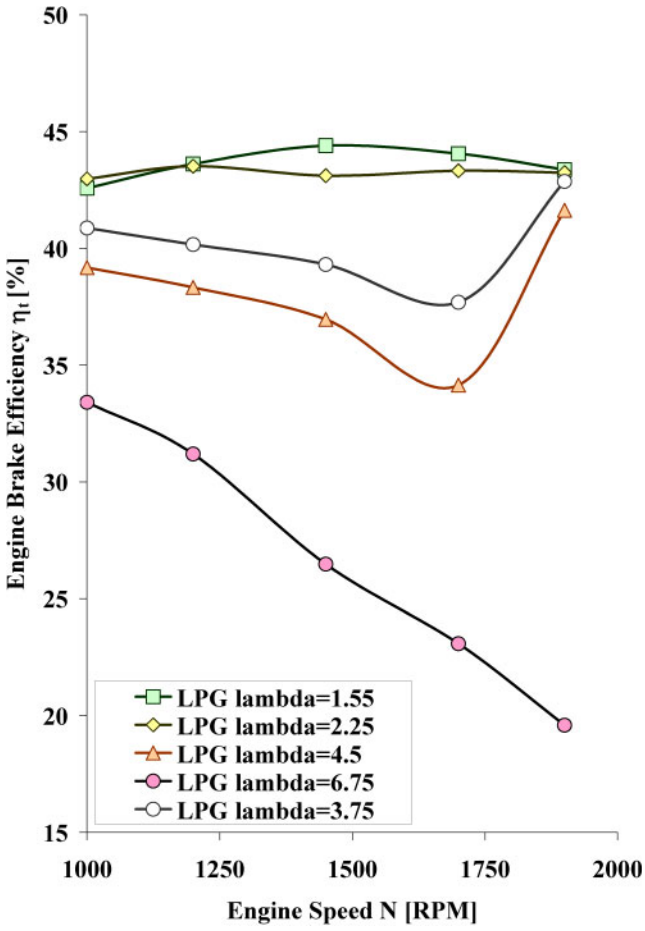

Fig. 19 Computed brake efficiency for the LPG-fuelled truck engine with various λ values from 1.55 to 6.75

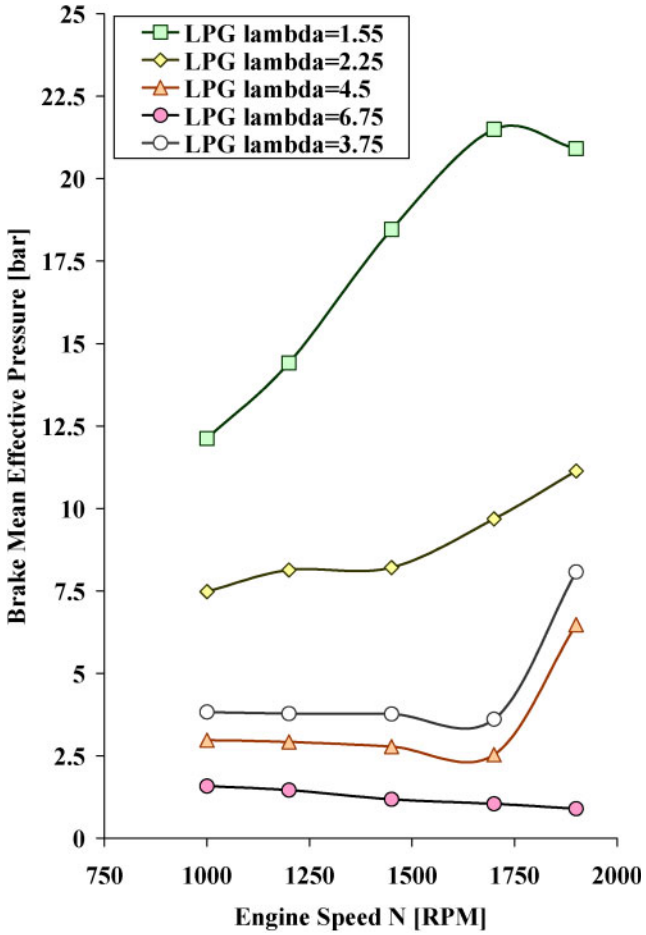

Fig. 20 Computed BMEP for the LPG-fuelled truck engine with various λ values from 1.55 to 6.75

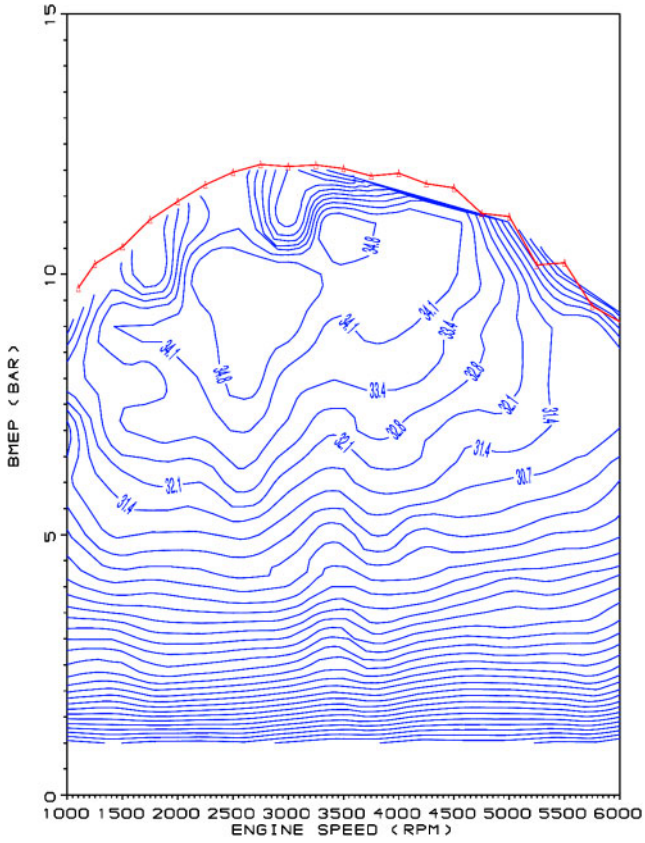

Fig. 21 Computed brake efficiency map of a 4-l, naturally aspirated, stoichiometric gasoline engine for a passenger car (BMEP versus engine speed for various brake efficiencies (per cent))

the brake efficiency and BMEP results respectively for the LPG engine with various air-to-fuel equivalence ratios. The DI-JI LPG engine has an almost constant brake efficiency exceeding 40 per cent from one third to full load. Use of air-to-fuel equivalence ratios smaller than $\lambda = 2.25$ could in principle allow Euro 6 emission standards to be met for NO_x without after-treatment, but at the expense of low BMEP outputs.

Figure 21 presents the brake efficiency map of a passenger car gasoline engine as a reference. The naturally aspirated in-line six-cylinder engine having a displacement of 4 l and a CR of 10:1 is running stoichiometric with load control by throttling the intake. The range of engine speeds covered is up to 6000 r/min. Figures 22 and 23 present the brake efficiency maps of the 11-l, turbocharged, in-line six-cylinder truck diesel and LPG engines respectively. The range of engine speeds covered is up to 1900 r/min. Owing to the higher CR, the partial recovery of exhaust energy, the lean operation, the load control by quantity of fuel injected, and the operation over a reduced range of engine speeds, the diesel and LPG engines have much larger top brake efficiencies and part-load efficiencies. The converted LPG engine has a much better part-load operation than that of the diesel egine and has a BMEP of 5 bar obtained with $\lambda = 2.25$–3.75 and brake efficiencies of around 40 per cent. While the diesel truck and gasoline passenger car models are validated versus engine dynamometer data, the LPG truck model is not validated because the DI-JI engine concept is still in a preliminary stage with funding for prototyping and experimental testing still unavailable. However, considering that the predicted fast rates of combustion of the DI-JI engine concept are in line with previous experiments with inhomogeneous charge [**19**] and homogeneous charge [**15–21**] configurations, they are therefore quite reliable; the brake efficiency predictions just follow these fast rates of combustion and share their reliability. The predicted top brake efficiencies, but even more so the predicted part-load efficiencies of the DI-JI LPG engine, are very significant, because they show the opportunity to achieve not only the diesel top brake

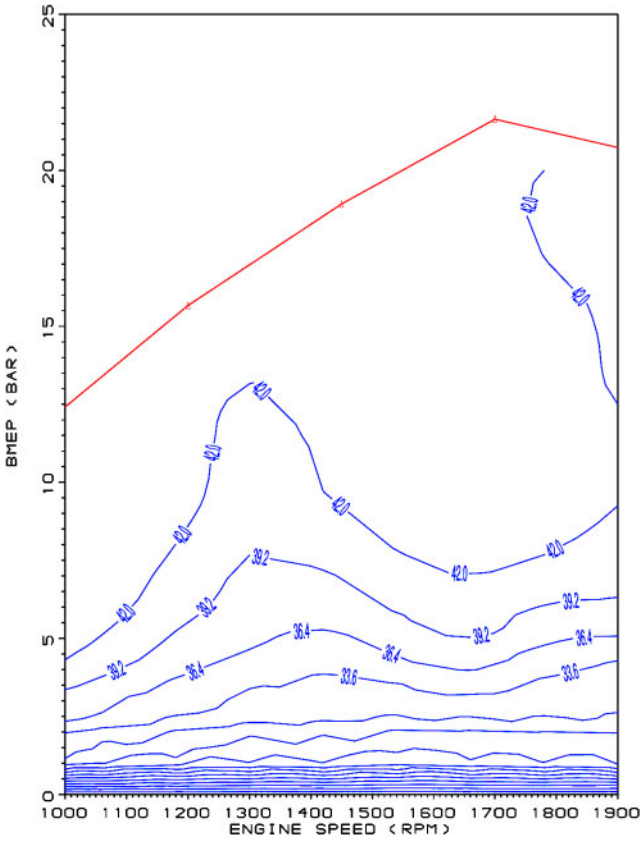

Fig. 22 Computed brake efficiency map of the 11-l turbocharged lean-burn diesel engine for a heavy-duty truck (BMEP versus engine speed for various brake efficiencies (per cent))

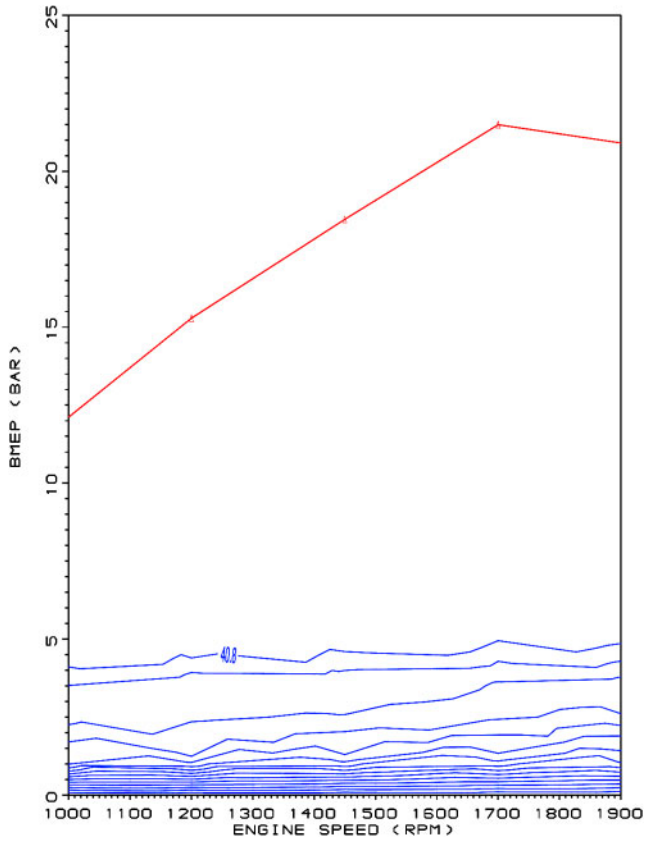

Fig. 23 Computed brake efficiency map of the 11-l turbocharged lean-burn diesel engine for a heavy-duty truck converted to LPG (BMEP versus engine speed for various brake efficiencies (per cent))

efficiencies but also the diesel part-load brake efficiencies on igniting with reacting jets controlled by a spark discharge to produce a slightly lean mixture within part of the in-cylinder volume.

5 CONCLUSIONS

Development of a JI pre-chamber is central to the development of always-lean-burn engines, where the load can be controlled by the quantity of fuel injected within the main chamber by a DI fuel injector and then bulk ignited by multiple jets of hot reacting gases.

Stand-alone pre-chamber and pre-chamber-plus-in-cylinder CFD simulations and CAE engine simulations as well as the analogous experiments should all be considered in the development of the many devices covered by the DI-JI engine concept because of their complementarities and different levels of complexity and different details.

The JI pre-chamber has many advantages over a standard spark plug main-chamber ignition. This ignition system can be used with or without DI, in the latter case to burn mixtures much leaner or just to burn the same mixtures more quickly with larger bores. Coupled with DI, JI allows bulk ignition of stratified mixtures, and therefore bulk combustion far from the solid boundaries, thus avoiding large heat losses. High-energy ignition by a large quantity of hot, partially burned combustion products in multiple locations across the main combustion chamber greatly enhances the rate of combustion when reference is made to a standard pointwise limited energy spark ignition.

By carefully optimizing the main-chamber injector location and geometric and operation parameters, the in-cylinder geometry including the bowl-in-piston shape, the ignition pre-chamber injector location, the geometric and operation parameters, the ignition pre-chamber spark plug location, the ignition pre-chamber geometry and location with reference to the in-cylinder volume also including the number and orientation of nozzles, the system may produce extremely efficient combustion over

the full range of engine loads as well as a significant increase in the top brake efficiencies of flame front propagating engines.

New engines fully designed to accommodate DI and JI ignition may have efficiencies exceeding 50 per cent running lean with C_3H_8 and H_2 fuels. Conversion of existing diesel truck engines to run C_3H_8 fuels with replacement of the diesel DI fuel injector with the DI fuel injector of LPG and a JI prechamber may improve efficiencies by up to 2 per cent at high speeds and may permit brake efficiencies of 42–44 per cent over all the range of engine speeds from one third to full load.

The benefits of the technology include reduced greenhouse and other emissions and reduced consumption as well as encouraging the increased uptake of alternative fuels, thus potentially enhancing national energy security and reducing greenhouse gas emissions. This work, which is still in progress, is aimed at reducing and capturing emissions in transport and energy generation, with particular emphasis to conversion of high-duty diesel engines to run gaseous fuels, with the goal of achieving Euro 6 emission standards without after-treatment (but obviously a very different specific power of the thermal engine). Exhaust energy recovery, heat insulation, engine buffering, charge cooling, and cooled exhaust gas recirculation, which are not considered here, may be relevant to achieving better efficiencies while meeting Euro 6 emission standards.

ACKNOWLEDGEMENTS

The authors wish to thank Tom Morel of Gamma Technologies Inc., Peter Ewing of VETA Pty Ltd and CD-adapco Australia, and Harry C. Watson for the support provided.

REFERENCES

1 Bureau of Infrastructure, Transport and Regional Economics, Australian Government, Road and rail freight: competitors or complements. Information Sheet 34, DOTARS ID 08470, July 2009, available from http://www.bitre.gov.au/publications/23/Files/IS34_RoadRailFreight.pdf (accessed 1 January 2010).

2 Department of Climate Change and Energy Efficiency, Australian Government, Australia's national greenhouse gas inventory: update quarterly estimates of Australia's national inventory: March quarter 2009, available from http://www.climatechange.gov.au/inventory/2007/pubs/quarterly-updatenggi.pdf (accessed 1 January 2010).

3 **Beer, T., Grant, T., Brown, R., Edwards, J., Nelson, P., Watson, H.,** and **Williams, D.** Life-cycle emissions analysis of alternative fuels for heavy vehicles: stage 1, CSIRO Atmospheric Research Report C/0411/1.1/F2 to the Australian Greenhouse Office, Department of the Environment, Water, Heritage and the Arts, Australian Government, March 2000, available from http://www.environment.gov.au/settlements/transport/publications/pubs/lifecycle.pdf (accessed 8 July 2010).

4 **Beer, T., Grant, T., Morgan, G., Lapszewicz, J., Anyon, P., Edwards, J., Nelson, P., Watson, H.,** and **Williams, D.** Comparison of transport fuels final report (EV45A/2/F3C) to the Australian Greenhouse Office on the stage 2 study of life-cycle emissions analysis of alternative fuels for heavy vehicles, Australian Government, Department of the Environment, Water, Heritage and the Arts, 2008, available from http://www.environment.gov.au/settlements/transport/comparison/pubs/comparison.pdf (accessed 1 January 2010).

5 US Department of Energy, Energy efficiency and renewable energy, vehicle technology program, 'FY 2008 progress report for advanced combustion engine technologies', 2008, available from http://www1.eere.energy.gov/vehiclesandfuels/pdfs/program/2008_adv_combustion_engine.pdf (accessed 1 January 2010).

6 Delphi, Worldwide emission standards: heavy duty and off-road vehicles, 2009, available from http://www.delphi.com/pdf/emissions/Delphi-Heavy-Duty-Emissions-Brochure-2009.pdf (accessed 8 July 2010).

7 **Boretti, A. A.** and **Watson, H. C.** *Lean-burn direct injection jet ignition internal combustion engine.* IP Aust. Provisional Pat. Appl. SPEP-11865853 (2009901639), 17 April 2009.

8 **Boretti, A., Watson, H.,** and **Tempia, A.** Computational analysis of the lean-burn direct-injection jet ignition hydrogen engine. *Proc. IMechE, Part D: J. Automobile Engineering*, 2010, **224**(2), 261–269. DOI: 10.1243/09544070JAUTO1278.

9 **Boretti, A. A.** and **Watson, H. C.** *Lean-burn direct injection jet ignition internal combustion engine without spark plug.* IP Aust. Provisional Pat. Applic. SPEP-11928154 (2009901961), 5 May 2009.

10 **Boretti, A. A.** and **Watson, H. C.** Development of a direct injection high efficiency liquid phase LPG spark ignition engine. In Proceedings of the SAE 2009 International Powertrains, Fuels and Lubricants Meeting, Florence, Italy, 15–17 June 2009, SAE paper 2009-01-1881, 2009.

11 **Boretti, A. A.** and **Watson, H. C.** Development of a direct injection high flexibility CNG/LPG spark ignition engine. In Proceedings of the SAE 2009 International Powertrains, Fuels and Lubricants Meeting, Florence, Italy, 15–17 June 2009, SAE paper 2009-01-1969, 2009.

12 **Boretti, A. A.** and **Watson, H. C.**. The lean-burn direct-injection jet-ignition turbocharged liquid phase LPG engine. In Proceedings of the 15th Asia Pacific Automotive Engineering Conference (*APAC 15*), Hanoi, Vietnam, 26–28 October 2009 (Cultural & Communication Publisher, Aanoi, Vietnam).

13 **Boretti, A.** and **Watson, H. C.** The lean-burn direct-injection jet-ignition gas engine. *Int. J. Hydrogen Energy*, 2009, **34**, 7835–7841.

14 **Boretti, A.** and **Watson, H. C.** The lean-burn direct-injection jet-ignition flexi gas fuel LPG/CNG engine. In Proceedings of the 2009 SAE Powertrains, Fuels and Lubricants Meeting, San Antonio, Texas, USA, November 2009, SAE paper 2009-01-279, 2009.

15 **Lumsden, G., Watson, H. C., Glasson, N., Chow, C.,** and **Chalko, T.** Observations of hydrogen assisted jet ignition. In Proceedings of Hydrogen Power – Theoretical and Engineering Solutions – International Symposium (*HyPOTHESIS*), Gaeta, Italy, June 1995, vol. 1, pp. 433–443 (International Association for Hydrogen Energy, Miami, Florida).

16 **Lumsden, G.** and **Watson, H. C.** Optimum control of an S.I. engine with a $\lambda = 5$ capability. SAE paper 950689, 1995.

17 **Lumsden, G.** and **Watson, H. C.** HAJI operation in a hydrogen-only mode for emission control at cold start. SAE paper 950412, 1995.

18 **Lawrence, J.** *Hydrocarbon emission from a HAJI equipped ultra lean-burn engine.* PhD Thesis, University of Melbourne, Parkville, Melbourne, Australia, 1999.

19 **Dober, G.** *Geometric control of HC emissions.* PhD Thesis, University of Melbourne, Parkville, Melbourne, Australia, 2002.

20 **Hamori, F.** *Optimising the application of HAJI to the supercharged engine.* PhD Thesis, University of Melbourne, Parkville, Melbourne, Australia, 2006.

21 **Mehrani, P.** *Flame propagation and knocking in a HAJI engine.* PhD Thesis, University of Melbourne, Parkville, Melbourne, Australia, 2008.

22 NGK Spark Plug Europe, NGK glow plugs – you can rely on these, 2010, available from http://www.ngk.de/Glow_plugs.687.0.html (accessed 1 January 2010).

23 NIST Chemistry WebBook, 2008, available from http://webbook.nist.gov/ (accessed 1 January 2010).

24 Delphi, Delphi Multec® 20 GDi fast single coil fuel injector, 2009, available from http://delphi.com/shared/pdf/ppd/pwrtrn/gas_multec_gdifsc.pdf (accessed 1 January 2010).

25 VDO, available from http://www.conti-online.com/generator/www/de/en/continental/automotive/themes/passenger_cars/powertrain/engine_systems/engine_systems_en,tabNr=2.html (accessed 8 July 2010).

26 Hoerbiger, Ported fuel injectors for H_2 and CNG, 2009, available from http://www.hoerbiger.com/Niche-Automotive-Applications.10762.0.html (accessed 1 January 2010).

27 **Heindl, R., Eichlseder, H., Spuller, C., Gerbig, F.,** and **Heller, K.** New and innovative combustion systems for the H_2-ICE: compression ignition and combined processes. In Proceedings of the 2009 SAE World Congress, Detroit, Michigan, USA, 20–23 April 2009, SAE paper 2009-01-1421, 2009.

28 Delphi, Delphi Multec® 10 GDi multi-hole fuel injector, 2007, available from http://delphi.com/shared/pdf/ppd/pwrtrn/gas_multecdig_hom.pdf (accessed 1 January 2010).

29 NGK Spark Plugs (USA), Series of NGK racing spark plugs, 2010, available from http://www.ngksparkplugs.com/images/pdfs/racing_catalog.pdf (accessed 1 January 2010).

30 GT Gamma Technologies, available from http://www.gtisoft.com/products/p_GT_SUITE.php (accessed 8 July 2010).

31 Ricardo, available from http://www.ricardo.com/en-gb/Software/Products/WAVE/ (accessed 8 July 2010).

32 CD-adapco, STAR-CCM+ Product Information, 2010, available from http://www.cd-adapco.com/products/STAR-CCM_plus/ (accessed 1 January 2010).

33 DARS, What is DARS?, 2007, available from http://www.diganars.com/about.html (accessed 1 January 2010).

34 **Lehtiniemi, H.** Efficient engine CFD with detailed chemistry. In *Future Fuels for IC Engines*, Proceedings of the Engine Research Center 2007 Symposium, Madison, Wisconsin, USA, 6–7 June 2007, available from http://www.erc.wisc.edu/documents/symp07-Lehtiniemi.pdf (accessed 1 January 2010).

APPENDIX

Figures 24 and 25 present combustion pictures (from reference [**19**]) obtained at different crank angles ATDC. These combustion photographs of the six-jet HAJI engine with late side DI of C_4H_{10} have overlaid positions of injector, exhaust valves, and cylinder. The photographs in Fig. 24 are at 5°, 9°, 12°, 16°, 19°, and 23° crank angle ATDC ordered from left to right and from top to bottom with the engine operating at 1500 r/min, 0.11 g/s of C_4H_{10} fuel injected, and $\lambda = 2.3$. The photographs in Fig. 25 are at 2°, 7°, 11°, 14°, 18°, and 22° crank angle ATDC ordered from left to right and from top to bottom with the engine operating at 1500 r/min, 0.11 g/s of C_4H_{10} fuel injected, and $\lambda = 2.6$. Despite the large air-to-fuel ratio and the cold walls and charge, the combustion evolution is quite fast following the JI, even if only a few jets are directed towards the region where the fuel is available. Table 2 presents the combustion delays and durations with various fuelling strategies and spark timings for an engine speed of 1500 r/min and 0.11g/s of C_4H_{10} fuel

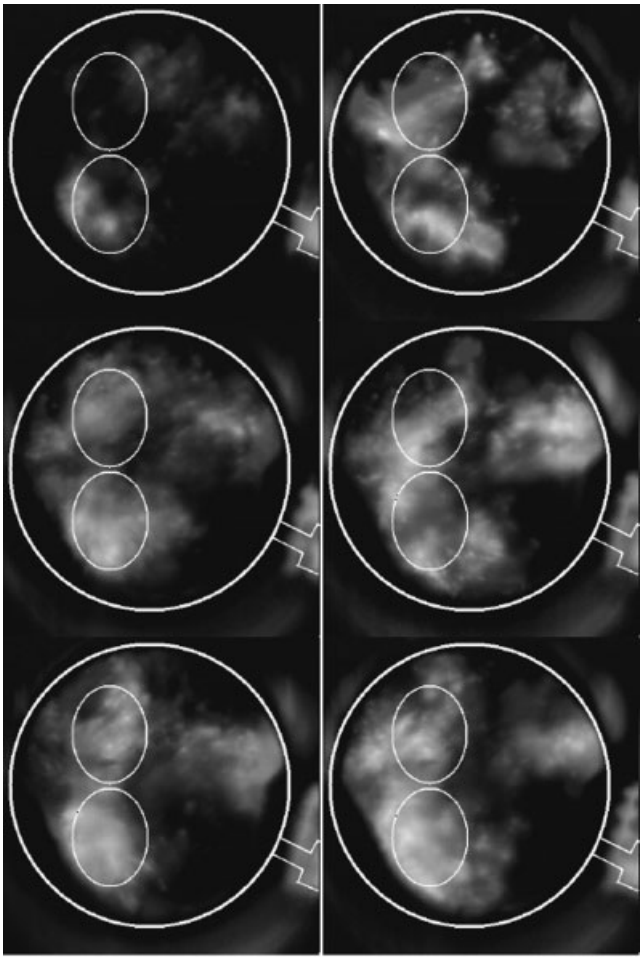

Fig. 24 Combustion photographs (from reference [**19**]) of a six-jet HAJI engine with late side DI of C_4H_{10} with overlaid positions of the injector, exhaust valves, and cylinder. The photographs are at 5°, 9°, 12°, 16°, 19°, and 23° crank angle ATDC ordered from left to right and from top to bottom with the engine operating at 1500 r/min, 0.11 g/s of C_4H_{10} fuel injected, and $\lambda = 2.3$

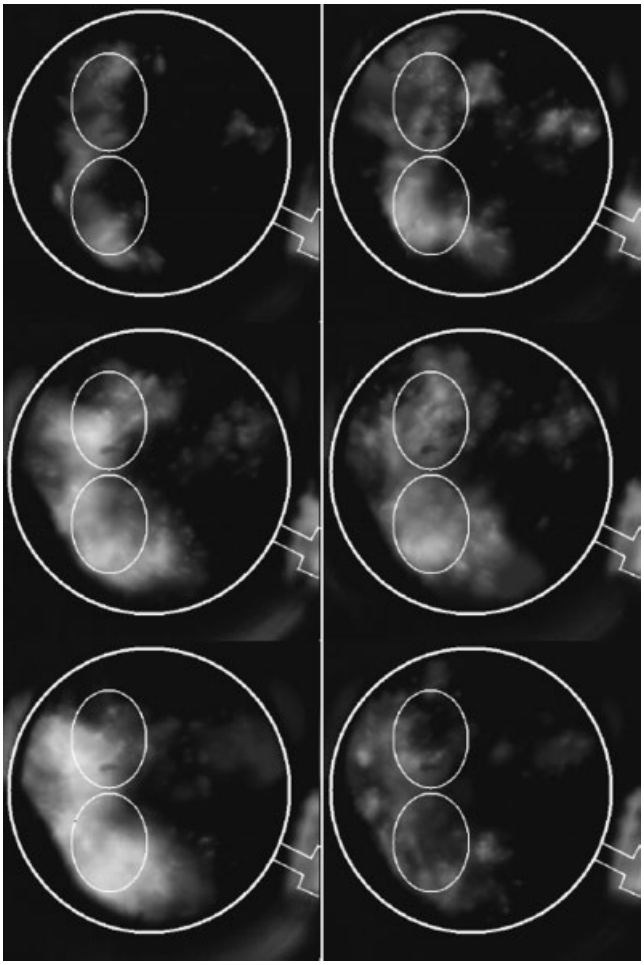

Fig. 25 Combustion photographs (from reference [**19**]) of a six-jet HAJI with late side DI of C_4H_{10} with overlaid positions of the injector, exhaust valves, and cylinder. The photographs are at 2°, 7°, 11°, 14°, 18°, and 22° crank angle ATDC ordered from left to right and from top to bottom with the engine operating at 1500 r/min, 0.11 g/s of C_4H_{10} fuel injected, and $\lambda = 2.6$

Table 2 Combustion delays and durations with various fuelling strategies and spark timings for an engine speed of 1500 r/min and 0.11 g/s of C_4H_{10} fuel injected (from reference [**19**])

Fuelling strategy	λ	Spark advance (deg CA)	0–5% mass fuel burned (deg CA)	5–95% mass fuel burned (deg CA)
PFI	1.2	6	11	36
	1.6	−4	6	41
	1.8	12	4	38
	2.1	28	5	41
	2.4	28	4	42
Early DI	1.2	12	7	17
	1.4	4	7	19
	1.9	20	4	27
	2.3	28	5	40
	2.7	36	5	59
Late DI	1.6	0	3	17
	2.0	4	3	20
	2.5	−4	4	28
	2.8	0	4	33
	3.4	−4	4	30

injected (from reference [**19**]). Side injection produces a richer mixture on the side opposite to the injector location. With reference to late DI, early DI reduces the charge stratification. Mixing of fuel and air is, however, less complete with early DI than with PFI. The HAJI pre-chamber was located at the centre of the spark plug delivering multiple jets of reacting gases over all the combustion chambers. Spark advances were close to maximum brake torque values.

Despite the poor atomization of the DI fuel injector spray and the side stratification of the spray in cold air close to cold walls where the combusting charge is finally ignited by only a few of the igniting jets, the combustion evolution appears to be much faster with late DI than with early DI and PFI. These preliminary results suggest the option to develop further the concept of an always-lean-burn engine coupling central DI with a good injector with central JI.